Annals of Biomedical Engineering, Vol. 32, No. 11, November 2004 (© 2004) pp. 1519–1529

Green's Function Methods for Analysis of Oxygen Delivery to Tissue by Microvascular Networks

TIMOTHY W. SECOMB,[1] RICHARD HSU,[1] ERIC Y. H. PARK,[2] and MARK W. DEWHIRST[2]

[1]Department of Physiology, University of Arizona, Tucson, AZ and [2]Department of Radiation Oncology, Duke University Medical Center, Durham, NC

(Received 7 April 2004; accepted 30 June 2004)

Abstract—Delivery of oxygen to tissue is an essential function of the circulatory system. The distance that oxygen can diffuse into oxygen-consuming tissue is small, and so tissue oxygenation is critically dependent on the spatial arrangement of microvessels in tissue. Theoretical methods have been developed to simulate the spatial distribution of oxygen levels in tissue surrounding a network of microvessels. Here, numerical methods based on a Green's function approach are presented, for realistic three-dimensional network geometries derived from observations of skeletal muscle, brain, and tumor tissues. Relative to finite-difference methods, the Green's function approach reduces the number of unknowns in the numerical formulation and allows rapid computations even for complex vascular geometries. Generally, the boundary conditions on the exterior of the computational domain are not known. Imposition of a no-flux boundary condition can lead to exaggerated estimates of the extent of hypoxia in the tissue region. A new version of the method is described that avoids this problem and can be applied to arbitrarily shaped tissue domains.

Keywords—Oxygen transport; Diffusion; Microvessels; Mathematical models.

INTRODUCTION

As a consequence of the relatively low solubility of oxygen in tissue, the maximum distance that oxygen can diffuse into oxygen-consuming tissue is small, typically in the range 20–100 μm.[34] Steep gradients in partial pressure of oxygen (PO_2) are necessary to provide sufficient diffusive fluxes to meet tissue needs. The microcirculation achieves this by providing an array of small, closely spaced blood vessels. Tissue oxygen levels are sensitively dependent on the spatial arrangement of these microvessels.

Measurements of PO_2 gradients on microscopic scales are technically difficult or impossible in many cases of interest, and understanding of oxygen transport in the microcirculation has relied heavily on theoretical approaches. In the classic model of Krogh,[23] which has provided the starting point for many subsequent developments,[25,27] the microcirculation is represented as an array of parallel, evenly spaced capillaries, and each capillary provides oxygen by diffusion to a concentric cylindrical region of tissue. The diffusive flux of oxygen across the outer surface of the cylinder is assumed to be zero. This model is most directly applicable to skeletal muscle, where capillaries generally run parallel to the muscle fibers. However, many features of oxygen transport in the microcirculation are not adequately described by models based on the Krogh cylinder concept. In skeletal muscle, for example, capillaries are not evenly spaced, and this affects oxygen levels.[18,22] Arterioles deliver a significant fraction of the oxygen demand in muscle under resting conditions.[8,31] In brain tissue, capillaries are curved and do not show a strong alignment in one direction.[32] The distribution of microvessels in tumor tissues is very heterogeneous, which results in the occurrence of hypoxic microregions.[34]

The need to simulate such phenomena has motivated the development of models using more realistic and complex vascular geometries than the Krogh cylinder. Popel[27] reviewed progress in this area up to about 1989. Subsequent work has used a variety of techniques. Secomb and Hsu[19,30] developed an approach in which each vessel is represented as a distribution of oxygen sources, within a defined tissue region. The tissue oxygen field is represented as a superposition of the fields resulting from these sources. The further development of this "Green's function" approach is the subject of the present study. Approaches based on similar principles were developed independently by Groebe,[13] considering each red blood cell as a discrete source of oxygen, and Hoofd *et al.*,[16,17] considering two-dimensional diffusion from irregularly spaced parallel capillaries. More recently, finite-difference methods have been used for three-dimensional problems by Goldman and Popel[10,11] and by Beard *et al.*,[2,3] and for two-dimensional problems by Lo *et al.*[24]

Our Green's function method[19] has been used for the simulation of oxygen transport in tumors,[33,34] skeletal

Address correspondence to T. W. Secomb, PhD, Department of Physiology, University of Arizona, Tucson, AZ 85724-5051. Electronic mail: secomb@u.arizona.edu

0090-6964/04/1100-1519/1 © 2004 Biomedical Engineering Society

muscle,[31] and brain.[32] In the course of these studies, several modifications were made. For cases involving occurrence of hypoxia, the method was modified to take into account the nonlinear dependence of tissue oxygen consumption on local PO_2 in hypoxic regions.[31,34] Estimates of the extent of hypoxia in such cases were found to depend significantly on the choice of boundary conditions on the tissue domain. The original choice of a no-flux boundary condition is not necessarily optimal, and an alternative approach was proposed by Secomb *et al*.[32] As originally developed, the method was restricted to rectangular cuboidal tissue domains. The objective of this study is to provide a systematic development of the Green's function method, and to present a new version that avoids the use of a no-flux boundary condition and can be applied to tissue domains of arbitrary shape.

METHODS

Governing Equations

The tissue is represented as a homogeneous medium with respect to oxygen transport, with uniform oxygen diffusivity D and solubility α. The vessel walls are treated as part of the tissue space. Steady-state conditions are assumed. Fick's law of diffusion and the principle of conservation of mass lead to the governing equation

$$D\alpha\nabla^2 P = M(P) \tag{1}$$

where P is the tissue PO_2, $M(P)$ is the consumption rate, and ∇^2 is the Laplacian operator. In many cases of interest, the PO_2 falls to low values and oxygen consumption is limited by oxygen availability. The dependence of consumption on PO_2 is represented by a Michaelis–Menten relationship

$$M(P) = M_0 P/(P_0 + P) \tag{2}$$

where M_0 represents the oxygen demand, i.e., the rate of oxygen consumption when oxygen supply is not limiting and P_0 represents the PO_2 at half-maximal consumption. In the results presented here, M_0 is assumed to be uniform, but regional variations in oxygen demand could readily be incorporated into simulations using this method.

The boundary conditions on the outer surface of the tissue region are frequently not determined by available experimental information, and additional assumptions must be made so that the problem is completely specified. Analogy with the Krogh cylinder model suggests imposing a no-flux boundary condition. Imposing periodic boundary conditions represents a second possible choice. When the problem is formulated using a Green's function approach, a further possibility exists: the tissue region can be considered as embedded in an effectively infinite domain with the same diffusivity, containing no oxygen sources and sinks outside the specified tissue region.[13] This leads to a well-posed problem, without imposing an explicit boundary condition on the outer surface of the tissue region. The advantages and disadvantages of these approaches are discussed below (see Discussion).

The rate of convective oxygen transport along a vessel segment is given by

$$f(P_\mathrm{b}) = Q(H_\mathrm{D} C_0 S(P_\mathrm{b}) + \alpha_\mathrm{eff} P_\mathrm{b}) \tag{3}$$

where Q is the flow rate of blood, H_D is the discharge hematocrit, S is the oxyhemoglobin saturation, P_b is the blood PO_2, C_0 is the concentration of hemoglobin-bound oxygen in a fully saturated red blood cell and α_eff is the effective solubility of oxygen in blood. In general, P_b varies with position along a segment. Both Q and H_D may be assumed constant along a given segment but may vary from one segment to another. The discharge hematocrit H_D gives the volume flux of red blood cells as a fraction of the total volume flux in a vessel and therefore determines convective transport rates. Variations in H_D result from unequal partition of hematocrit at diverging bifurcations.[29] The oxyhemoglobin saturation is represented by the Hill equation:

$$S(P_\mathrm{b}) = P_\mathrm{b}^n \big/ \left(P_\mathrm{b}^n + P_{50}^n\right) \tag{4}$$

where P_{50} is the PO_2 at 50% saturation and n is a constant. The effective solubility of oxygen in blood is $\alpha_\mathrm{eff} = (1 - H_\mathrm{D})\alpha_\mathrm{p} + H_\mathrm{D}\alpha_\mathrm{rbc}$, where α_p and α_rbc are the solubilities in plasma and red blood cells, respectively. Under normal conditions, the contribution of dissolved oxygen to convective oxygen transport is small, but it can be significant if blood PO_2 is very high or if hematocrit is very low. The values of α_p and α_rbc are similar[15] and so α_eff depends only slightly on hematocrit and can be approximated by a constant value. Conservation of oxygen implies that

$$df(P_\mathrm{b})/ds = -q_\mathrm{v}(s) \tag{5}$$

in each vessel segment, where s is distance along the segment, and q_v is the rate of diffusive oxygen efflux per unit vessel length.

At the interface between blood and tissue, the diffusive oxygen flux across the interface and the PO_2 must be continuous. For the diffusive flux, this implies that

$$q_v(s) = -D\alpha \int_0^{2\pi} \frac{\partial P}{\partial r} r_\mathrm{v}\, d\theta \tag{6}$$

where the vessel is assumed to be cylindrical, r is radial distance from the vessel centerline, r_v is the vessel radius and the integral is around the circumference, denoted by angle θ. Radial gradients in PO_2 are present also within microvessels, so P_b, the blood PO_2 appearing in Eq. (3), is considered as an effective average value over the vessel cross-section. For a vessel that is delivering oxygen, it exceeds the local tissue PO_2 at the interface with the blood. This relationship can be represented by the following equation, following Hellums[14]:

$$P_\mathrm{v}(s) = P_\mathrm{b}(s) - K q_\mathrm{v}(s) \tag{7}$$

where $P_v(s)$ is the tissue PO_2 averaged around the circumference of the vessel and K represents intravascular resistance to radial oxygen transport. Radial transport of oxygen within blood vessels is a complex process,[15] but we assume here that K is a constant that depends only on the vessel diameter.

If effects of myoglobin-facilitated diffusion of oxygen in tissue are of interest, they can be included by replacing P with P^* on the left-hand side of Eq. (1) and the right-hand side of Eq. (6) only, where P^* is the myoglobin-facilitated PO_2 defined by[9]

$$P^* = P + D_{Mb}C_{Mb}V_m S_{Mb}(P)/(D\alpha) \tag{8}$$

Here, D_{Mb} is the diffusion coefficient of myoglobin, C_{Mb} is its concentration, $S_{Mb}(P) = P/(P + P_{Mb50})$ is its oxygen saturation, P_{Mb50} is the PO_2 at half-maximal myoglobin saturation, and V_m is the molar volume.

Green's Function Formulations

The essential idea of the Green's function approach is to represent blood vessels as a set of discrete oxygen sources, and to represent the PO_2 field in the tissue as a superposition of fields resulting from those sources. If the rate of oxygen consumption in the tissue is known, the only unknowns in the problem are then the strengths of these sources. In the more general case in which oxygen consumption depends on PO_2, as in Eq. (1), the tissue region is represented as a set of discrete oxygen sinks, whose strengths are also unknowns in the problem.

According to potential theory,[20] the Green's function $G(\mathbf{x}; \mathbf{x}^*)$ for a given domain may be defined as the potential (i.e., the PO_2) at a point $\mathbf{x}$ resulting from a unit point source at $\mathbf{x}^*$, i.e., as the solution to

$$D\alpha\nabla^2 G = -\delta_3(\mathbf{x} - \mathbf{x}^*) \tag{9}$$

where δ_3 represents the three-dimensional delta function. The potential is then given by

$$P(\mathbf{x}) = \int_{\text{Sources}} G(\mathbf{x}; \mathbf{x}^*) q(\mathbf{x}^*)\, d\mathbf{x}^* \tag{10}$$

where $q(\mathbf{x})$ represents the distribution of source strengths. In an infinite domain, the solution is the singular function

$$G = G_1 = 1/(4\pi D\alpha|\mathbf{x} - \mathbf{x}^*|) \tag{11}$$

In a finite domain, additional, nonsingular terms may be needed to satisfy conditions imposed on the domain boundaries, as discussed below.

To a first approximation, the oxygen field resulting from oxygen diffusion from a long narrow vessel can be represented as the field resulting from a distribution of sources along the vessel centerline. However, this may not accurately represent the oxygen field close to the vessel, if it is assumed that the distribution source strength on the centerline is equal to the diffusive flux $q_v(s)$ as defined by Eq. (6). In an effort to obtain an improved representation, Hsu and Secomb[19] assumed that the oxygen source at each position along the vessel axis was uniformly distributed around the circumference of the vessel on the blood-tissue boundary. Recently, Pozrikidis[28] pointed out that in order to satisfy a flux boundary condition, not only a distribution of sources but also a distribution of dipoles on the surface is generally required, and that the method of Hsu and Secomb[19] itself represents an approximation.

To assess the errors resulting from these approximations, it is helpful to compute the actual distribution of diffusive flux across the vessel wall resulting from a given distribution of source strength along the vessel. For simplicity, a straight cylindrical segment of length L and radius r_0 in an infinite domain is considered, where $r_0 \ll L$. For each method used, the actual diffusive flux at the blood–tissue boundary can be expressed as

$$q_v(s) = \int_0^L F(s - s^*)\, q_0(s^*)\, ds^* \tag{12}$$

where $q_0(s)$ is the given distribution of source strength per unit length. In the case where distributions of both sources and dipoles are used,[28] $q_v(s) = q_0(s)$ and so $F(s) = \delta_1(s)$, the one-dimensional delta function. For sources distributed on the centerline, it is easily shown that $F(s) = \frac{1}{2}r_0^2 (s^2 + r_0^2)^{-3/2}$. For sources uniformly distributed around the circumference,[19]

$$F(s) = \frac{1}{2}\delta_1(s) + (4\pi r_0)^{-1} k[K(k) - E(k)] \tag{13}$$

In Eq. (13), $K(k)$ and $E(k)$ are the complete elliptic integrals of the first and second kinds, defined by

$$K(k) = \int_0^{\pi/2} (1 - k^2 \sin^2\theta)^{-1/2}\, d\theta \quad \text{and}$$

$$E(k) = \int_0^{\pi/2} (1 - k^2 \sin^2\theta)^{1/2}\, d\theta \tag{14}$$

where $k^2 = (1 + s^2/4r_0^2)^{-1}$. The function $F(s)$ in this case represents the distribution of radial flux across the cylindrical surface resulting from a unit source uniformly distributed around a circumferential ring at $s = 0$. Half of the flux from the source at any point on the circumference immediately exits the vessel, giving the contribution $\frac{1}{2}\delta_1(s)$ in Eq. (13). The other half passes through the vessel and exits as a distribution over the cylindrical surface. This distribution, when integrated with respect to the source point, gives the second term, which has a logarithmic singularity at $s = 0$. In the method of Pozrikidis,[28] the distribution of dipoles cancels the inward flux resulting from the distribution of sources.

As shown in Fig. 1, the function $F(s)$ decays rapidly with increasing $|s/r_0|$ in both approximations. For long slender vessels, with $r_0 \ll L$, it follows that $q_v(s) \approx q_0(s)$ except in regions where $q_0(s)$ has discontinuities or rapid

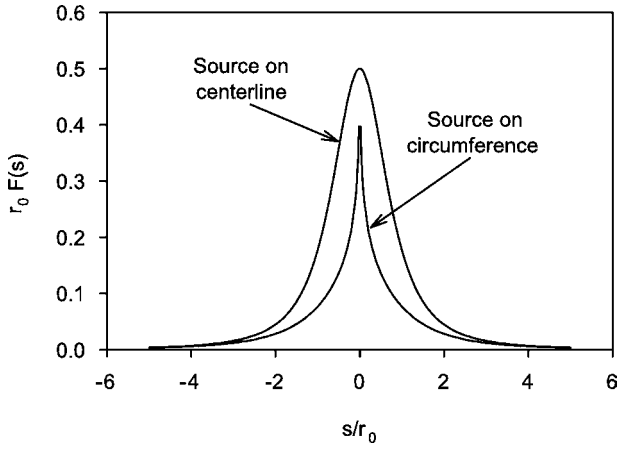

FIGURE 1. Normalized radial diffusive flux resulting from a point source at $s = 0$, on the centerline or distributed around the circumference, as a function of axial position. This is equivalent to the kernel function in Eq. (12) (see text). For the case when the source is distributed around the circumference, a delta function of weight $\frac{1}{2}$ is added to the function shown.

nonlinear changes. For example, significant discrepancies may arise near the ends of a finite-length vessel segment.[28] However, for cases relevant to oxygen transport, segments are generally connected to other segments, giving continuous, smoothly varying oxygen sources, and the errors resulting from use of the approximate forms are smaller than the errors resulting from the discretization used in the numerical solution of the problem. In the simulations presented here, the approach of Hsu and Secomb[19] will be retained.

Numerical Methods

Vessels are discretized into m short segments and the tissue space is discretized into n small approximately cubic regions. An $m \times m$ matrix of influence coefficients is defined, in which the element G_{ij}^{vv} is the average tissue PO_2 at the surface of vessel segment i resulting from a unit source distributed on the surface of segment j. It is derived from the Green's function $G(\mathbf{x}; \mathbf{x}^*)$ by integrating with respect to both $\mathbf{x}$ and $\mathbf{x}^*$ over the surfaces of the appropriate vessel segments. In practice, this integration is needed only for diagonal elements of the matrix. For off-diagonal elements, which represent the PO_2 at one segment resulting from a unit source at a different segment, G_{ij}^{vv} may be approximated by evaluating $G(\mathbf{x}; \mathbf{x}^*)$ at the midpoints of the two segments. An $n \times n$ matrix is defined in which the element G_{ij}^{tt} is the average tissue PO_2 in tissue region i resulting from a unit source distributed over tissue region j, and its off-diagonal elements may be similarly approximated. An $m \times n$ matrix is formed of the coefficients G_{ij}^{vt}, defined as the tissue PO_2 at the midpoint of vessel segment i resulting from a unit source at the midpoint of tissue region j, and an $n \times m$ matrix is formed of the coefficients G_{ij}^{tv}, defined as the tissue PO_2 at the midpoint of tissue region i resulting from a unit source at the midpoint of vessel segment j.

According to these definitions and using the Green's function representation, Eq. (10), the average PO_2 at the blood tissue interface of segment i and the average PO_2 in tissue region i are given respectively by

$$P_{v,i} = \sum_{j=1}^{m} G_{ij}^{vv} q_j + \sum_{j=1}^{n} G_{ij}^{vt} \varphi_j + G_0 \quad \text{for} \quad i = 1, \ldots, m \tag{15}$$

$$P_{t,i} = \sum_{j=1}^{m} G_{ij}^{tv} q_j + \sum_{j=1}^{n} G_{ij}^{tt} \varphi_j + G_0 \quad \text{for} \quad i = 1, \ldots, n \tag{16}$$

where q_j represents the source strength of segment j and ϕ_j represents the (negative) source strength of tissue region j. From Eq. (7),

$$P_{v,i} = P_{b,i} - K q_i \quad \text{for} \quad i = 1, \ldots, m \tag{17}$$

where $P_{b,i}$ is the PO_2 of blood at the midpoint of segment i. From Eq. (2),

$$\phi_j = -M(P_{t,j}) = -M_0 P_{t,j}/(P_0 + P_{t,j}) \quad \text{for} \quad j = 1, \ldots, n \tag{18}$$

where P_j represents the PO_2 in tissue region j as given by Eq. (16). The constant G_0 is required when the Green's function is arbitrary up to an additive constant, as is the case if no-flux boundary conditions are applied to the tissue domain, or if no boundary conditions are imposed. It is determined by the additional condition that the net oxygen delivery is equal to the consumption:

$$\sum_{j=1}^{m} q_j + \sum_{j=1}^{n} \varphi_j = 0 \tag{19}$$

By integrating Eq. (5), the rate of convective oxygen transport along vessel segment i at its midpoint, $f(P_{bi})$, can be expressed as a linear function of the source strengths q_j:

$$f(P_{bi}) = f\left(P_{bi}^0\right) - \sum_{j=1}^{m} \alpha_{ij} q_j \quad \text{for} \quad i = 1, \ldots, m \tag{20}$$

Here, P_{bi}^0 is the intravascular PO_2 of segment i in the absence of diffusive oxygen exchange (i.e, if $q_j = 0$ for all j), and is typically given by the assumed PO_2 of an upstream vessel as it enters the tissue domain. For a series of segments forming an unbranched vessel, α_{ij} takes the value 1 if segment j is upstream of segment i, $\frac{1}{2}$ if $i = j$, and 0 otherwise. For segments forming a branched network, the values of α_{ij} depend on the partition of oxygen fluxes at diverging bifurcations and the summation of fluxes at converging bifurcations. Because of the nonlinear form of

f according to Eq. (3) and the unequal partition of hematocrit at diverging bifurcations, the fractional partition of convective flux into two components at such bifurcations is (weakly) dependent on the PO_2. During the iterative solution (as described below), the values of α_{ij} are accordingly updated.

Eqs. (15), (17), and (20) may be combined to give a set of m equations to be solved together with Eq. (19) for q_j and G_0:

$$\sum_{j=1}^{m} G_{ij}\, q_j + G_0 - f^{-1}\left[f\left(P_{\mathrm{b}i}^{0}\right) - \sum_{j=1}^{m} \alpha_{ij} q_j \right] + K q_i = -\sum_{j=1}^{n} G'_{ij}\, \varphi_j \quad \text{for} \quad i = 1, \ldots, m \tag{21}$$

A two-level iterative procedure is used to solve this system. Initial estimates of tissue oxygen levels and vessel source strengths are defined, and the tissue source strengths ϕ_j are computed using Eq. (18). The inner iterative procedure is used to compute q_j and G_0 for given values of ϕ_j. The left-hand side of Eq. (21) is linearized about the current values of q_j, and the resulting linear system is solved together with Eq. (19) using the biconjugate gradients stabilized method,[36] giving updated values for q_j and G_0. The procedure is repeated using these updated values until convergence to a specified criterion is achieved. For the outer iteration, updated tissue oxygen levels are computed from Eq. (16) and used to update ϕ_j, and the inner iteration is repeated. The outer iteration is continued until convergence is achieved, usually within several steps. The outer iteration is not needed if the tissue is well-oxygenated and oxygen consumption can be assumed to be a known constant. The choice of iterative scheme for this problem is critical. In the method presented here, source strengths and oxygen levels of each vessel segment are solved for simultaneously, taking into account the dependence of intravascular PO_2 on the upstream source strengths. Simpler schemes in which one of these quantities is computed using values of the other from the previous iteration do not exhibit satisfactory convergence.

As mentioned earlier, the tissue space must be discretized if the consumption rate is dependent on PO_2, as in Eq. (1). This adds to the number of unknowns in the problem. In essence, the tissue mesh is used to approximate the right-hand side of a Poisson equation, $\nabla^2 P = g$. It can easily be shown, e.g., by using Fourier analysis, that inclusion of components of g with high spatial frequencies produce relatively small changes in P, compared to low frequency components with similar amplitude. As a consequence, a relatively coarse mesh can be used for this purpose, without introducing significant errors in the resulting oxygen field. A much finer mesh would be needed if the oxygen field itself were to be represented adequately by such a mesh.

Boundary Conditions

The Green's function for a point source in an infinite domain is given by Eq. (11). If the domain is finite, the Green's function must generally be modified to satisfy additional boundary conditions. Furthermore, if the no-flux boundary condition is imposed on the Green's function, the point source must be balanced by a sink term to satisfy conservation of mass, which is achieved by replacing Eq. (9) with $D\alpha\nabla^2 G = -\delta(\mathbf{x} - \mathbf{x}^*) + 1/V$, where V is the volume of the domain. This method was applied in the case of a cuboidal tissue domain with no-flux boundary conditions by Hsu and Secomb.[19] The resulting modified Green's function was represented as $G = G_1 + G_2 + G_3$, where G_1 is given by Eq. (11), G_2 is a quadratic function of the Cartesian coordinates x_1, x_2, and x_3, and G_3 is a function of x_1, x_2, and x_3, which is represented a sum of three double Fourier series. The coefficients appearing in the expressions for G_2 and G_3 depend on the position of the source point $\mathbf{x}^*$. The coefficients of G_2 are determined by setting $G = G_1 + G_2$ and imposing the condition that the net diffusive flux across each of the six boundary planes is then zero. The coefficients of G_3 are chosen such that $G_1 + G_2 + G_3$ satisfies the no-flux condition at each point on the boundary. Because the Fourier series are necessarily truncated, this condition is satisfied approximately. In the following, this solution is referred to as the "pointwise no-flux solution."

For problems of practical interest, imposition of the no-flux boundary condition is not necessarily appropriate. Realistic vascular networks have irregular geometries and local oxygen fluxes can occur across any arbitrarily chosen boundary in the tissue. Imposition of the no-flux condition on domain boundaries can result in exaggeration of the amount of hypoxia in the tissue, as discussed below. Therefore, we consider alternative approaches in which this condition is not imposed. One such approach is to include only the singular part of the Green's function, i.e., to set $G = G_1$ as given by Eq. (11). This gives the solution for the case in which the tissue region is embedded in an infinite domain, with the PO_2 approaching a constant value at large distances from the tissue region. In this "infinite-domain solution," the total net flux of oxygen out of the tissue region is zero, according to Eq. (19). Avoidance of the need to impose a specific boundary condition on the boundary of the region surrounding the vascular network is a potential advantage of this solution method. Other advantages are that the tissue domain is not restricted to a cuboidal shape, and that omitting the term G_3 avoids the need to compute the coefficients in the double Fourier series. A FORTRAN implementation of the infinite-domain solution method is available online (See http://www.physiol.arizona.edu/secomb/greens.html). A further alternative simplified approach is to set $G = G_1 + G_2$ as defined above and impose the condition that the net diffusive flux across each of the six boundary

planes is zero. This "net no-flux solution" was previously used by Secomb *et al*.[32] Results for the pointwise no-flux, net no-flux, and infinite-domain solutions are compared below.

The tissue region supplied with oxygen by a vascular network is not necessarily well represented by a cuboidal region containing the network. In reality, a point in the tissue near the boundary of such a cuboidal region might be expected to receive oxygen from vessels outside the region, if there is no vessel within the simulated network close to that point. An alternative method to define the tissue region associated with a given network was therefore developed. The goal of this procedure was to approximate the minimal convex shape containing all tissue points lying within a specified distance L of a vessel in the network. Making the domain convex avoids the occurrence of unrealistic holes in the domain, at points where no vessel is nearby. A large set of vectors was defined such that any direction in space is approximated by a vector in the set. For each vector, a set of points representing all the vessel segments was orthogonally projected onto a line parallel to the vector. Any tissue point whose projection onto that line was more than a distance L outside the set of projected vessel points was excluded from the tissue domain. In effect, regions lying beyond a set of tangent planes to the final domain, normal to the vectors in the set, are successively removed by this procedure. By choosing a suitable set of direction vectors, the minimal convex set can be approximated to any desired accuracy. The oxygen field can then be computed using the infinite-domain solution as described above, with oxygen sinks at each tissue point lying within the convex tissue region.

Applications

The Green's function methods described above have been used to simulate oxygen transport from microvascular networks to tissue in skeletal muscle,[19,31] tumors,[33,34] and brain.[32] Details of the three-dimensional vascular network geometries considered and the other assumptions made are described in the cited references, and additional information is available online (See http://www.physiol.arizona.edu/secomb/network.html). Here, results are presented for observed network configurations as shown in Fig. 2. The tumor network geometry was derived from confocal microscopic observations of mammary carcinoma (R3230AC) implanted in a rat dorsal skin flap preparation.[7,33] The brain network geometry was obtained by analyzing paired scanning electron micrographs of vascular corrosion casts in the rat superficial cortex.[26,32] Oxygen transport in these geometries was simulated using the three types of boundary conditions defined earlier (pointwise no-flux, net no-flux, and infinite domain), with the same cuboidal tissue domain in each case. Hypoxic fractions, defined as fraction of tissue with PO_2 less than a defined level (1, 3, or 5 mmHg) were estimated based on computed PO_2 at each tissue point in the mesh as previously described.

The observations of the skeletal muscle network have not previously been reported. To measure red blood cell fluxes, the cremaster muscle was prepared in a standard fashion for intravital microscopy and placed onto a temperature-controlled optical stage mounted on a Carl Zeiss Axioline intravital microscope (Carl Zeiss, Hanover, MD). Red blood cells from a donor rat were fluorescently labeled with 1,1′-dioctadecyl-3,3,3′,3′-tetramethylindocarbocyanine perchlorate (DiI; Molecular Probes, Eugene, OR), using the method of Unthank *et al*.[35] The fluorescently labeled cells were administered to the test animal to yield a fluorocrit (fraction of labeled cells) of approximately 1%. The actual fluorocrit was verified by analyzing an aliquot of blood from the recipient using flow cytometry.[5,21] Observation of red blood cell movement through the network was facilitated by coadministering fluorescently labeled liposomes, to act as a blood marker.[21] Following administration of the red cells and liposomes, the vascular network was traced from a video monitor onto acetate sheets for later comparison with the confocal images. Each vessel segment was assigned an identifying number. Directions of flow for each vessel segment were also noted on the acetate sheets. Red cell fluxes along 62 distinct flow pathways through the network were determined by videotaping regions of interest for periods of 2–5 min. A timing signal was superimposed on the video images. Fluxes were determined by counting the number of labeled cells that traversed each pathway. A minimum of 50 cells was counted for each segment. The actual red cell flux was then determined by dividing the number counted by the fluorocrit, and was expressed in terms of red blood cells per second.

The vascular network geometry was determined by intravenous infusion of a rhodamine-labeled lectin (Vector Laboratories, Burlingame, CA) prior to euthanasia. The muscle tissue was excised from the animal, preserved in 4% paraformaldehyde, and visualized at 20× using a Nikon Optishot microscope (Nikon, Melville, NY) equipped with an InSIGHT laser scanning confocal unit (Meridian Instruments, Okemos, MI). The optical sections were 2 μm thick. The vascular network was reconstructed manually by evaluating consecutive sections to determine the three-dimensional coordinates of the end points and several intermediate points along the centerline of each vessel segment. Flow directions and red blood cell fluxes were assigned to each segment by comparing the confocal images with the acetate sheets. The resulting network [Fig. 2(C)] does not conform to a cuboidal region and oxygen transport was therefore simulated using the "infinite-domain solution," with the tissue region defined by the procedure described above with $L = 0$. The resulting

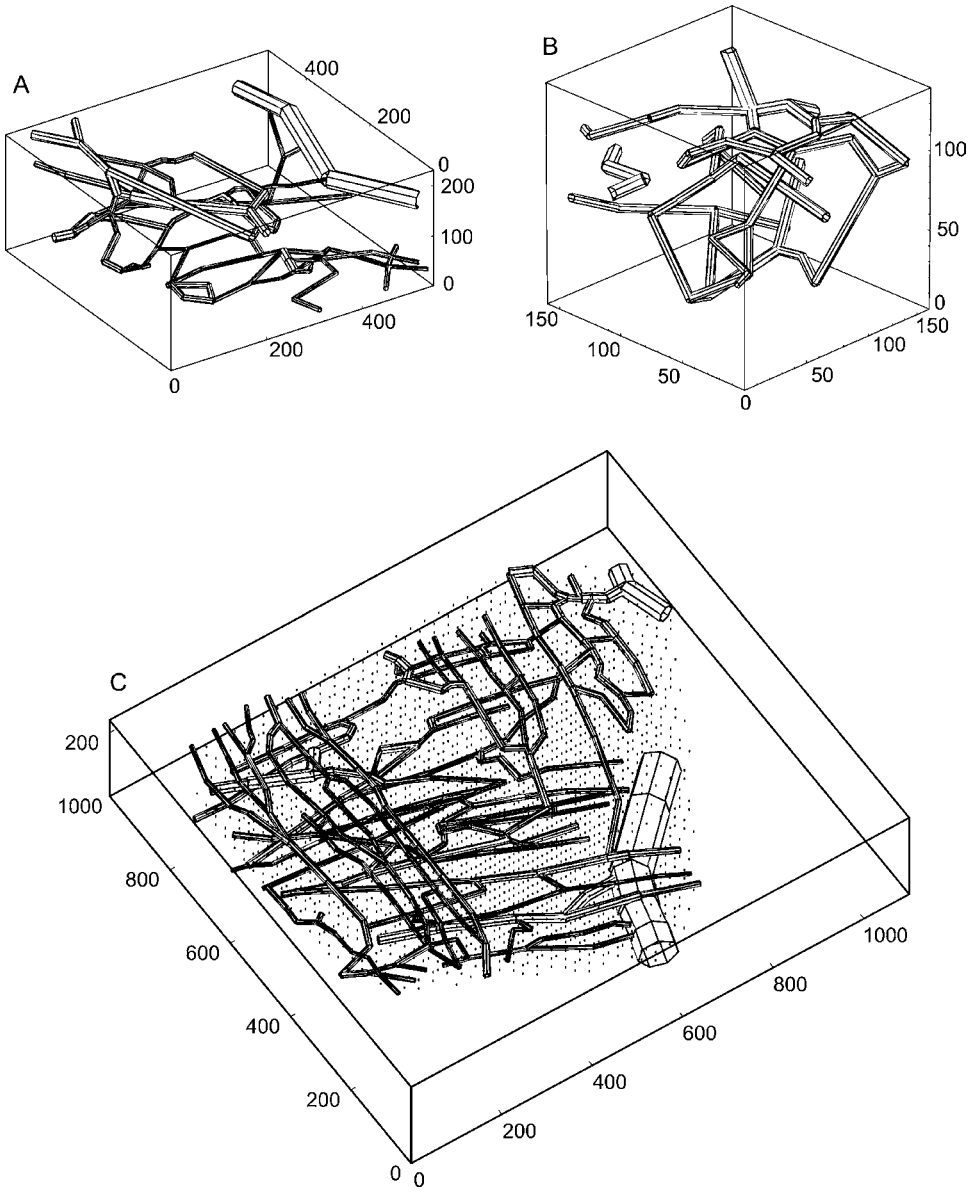

FIGURE 2. Vascular network configurations from observations in the rat, used in simulations. Dimensions are indicated in micrometer (μm). A. Tumor. B. Brain. C. Cremaster muscle; dots indicate the centers of tissue regions lying within the convex oxygen-consuming tissue domain associated with the vascular network. Each tissue region has an associated oxygen sink.

domain had a volume 25% of the volume of the surrounding cuboid.

Parameter Values

Parameter values specific to each vascular network are given in Table 1. These values are representative of realistic physiological conditions.[31,32,34] For simplicity, all inflowing vessels were assumed to have the same PO_2 although the method is not subject to this restriction. Different values of the Krogh diffusion coefficient ($D\alpha$) are used in each case, and are chosen for consistency with previous modeling studies for tumors,[34] brain,[32] and skeletal muscle[31] The estimate of $D\alpha$ for skeletal muscle is based on experiments carried out at body temperature,[4] whereas the values used for tumors and brain are based on extrapolations from lower temperatures and may underestimate the actual values. However, insufficient experimental data are available for these tissues to allow estimation of more accurate values. The hemoglobin-bound oxygen content of red blood cells at saturation is assumed to be $C_0 = 0.5$ cm^{3}O$_2$/cm^3 and the effective solubility of oxygen in blood is $\alpha_{\text{eff}} = 3.1 \times 10^{-5}$ cm^{3}O$_2$/cm^3/mmHg. Parameter values in the Hill equation for saturation are $n = 3$ and $P_{50} = 38$ mmHg for rats. The

TABLE 1. Parameter values used in simulations.

Tissue	Tumor	Brain	Cremaster[a]
Domain size (μm)	$550 \times 520 \times 230$	$150 \times 160 \times 140$	$1100 \times 1000 \times 240$
Number of vessel segments	104	50	295
Total vessel length (mm)	7.4	1.84	20.4
Number of subsegments	517	237	1170
Total blood flow to region (cm^3/s)	1.4×10^{-6}	1.8×10^{-7}	1.25×10^{-6}
Inflow PO_2 (mmHg)	40	50	50
Spacing of tissue points (μm)	30	10	30
Number of tissue points	2754	3360	10080
Oxygen consumption rate (cm^3O_2 $(100\ cm^3)^{-1}$ min^{-1})	1.5	14	4, 10
Krogh diffusion coefficient for oxygen (cm^3O_2 cm^{-1} s^{-1} $mmHg^{-1}$)	4.2×10^{-10}	6×10^{-10}	9.4×10^{-10}

[a] The computational domain was reduced according to the procedure described in the text; its volume is 25% of that of the surrounding cuboid.

values are typical of those found in many studies[6,12] Values of the parameter K, representing intravascular resistance to radial oxygen diffusion, were assumed to vary with vessel diameter, with $K = 3 \times 10^8$ mmHg cm s/cm^3O_2 in 4-μm vessels and $K = 9.3 \times 10^7$ mmHg cm s/cm^3O_2 in 33-μm vessels.[15,31] For skeletal muscle, oxygen consumption rates can vary over a wide range depending on the level of muscle activation. Simulations were performed at rates of 4 and 10 cm^3O_2 $(100\ cm^3)^{-1}$ min^{-1}, representative of mild and moderate levels of exercise.

RESULTS

Examples of computed PO_2 fields for tumor, brain, and skeletal muscle tissue are shown in Fig. 3, represented as contours in planar slices through the tissue domain. For the tumor and brain networks, solutions are presented for the three different types of boundary condition (pointwise no-flux, net no-flux, and infinite-domain). PO_2 levels in the central part of the domain are insensitive to the choice of boundary conditions, but some differences are evident in the regions near the tissue boundary. The effects of the choice of solution method on the predicted degree of hypoxia for the tumor and brain networks are shown in Table 2. In each case, the fraction of tissue that is hypoxic is reduced when the net no-flux and infinite-domain solutions are used, relative to the pointwise no-flux solution. For example, the predicted hypoxic fraction in the tumor tissue, based on PO_2 levels below 3 mmHg, is reduced from about 18% with the pointwise no-flux solution to about 10% when the infinite-domain solution is used. It should be noted that convective oxygen delivery and oxygen demand are unchanged in each case, and oxygen consumption increases slightly with decreases in hypoxic fraction. In the pointwise no-flux solution, the most hypoxic regions are generally predicted to occur near the corners of the tissue domain, suggestive of an artifact resulting from the no-flux boundary conditions. The reduction in predicted hypoxic fraction with the other two methods (Table 2) reflects increased predicted oxygen levels in these corner regions. In the infinite-domain solution, the reduction in overall hypoxic fraction is achieved as a result of oxygen fluxes that exit the tissue domain on some parts of the boundary and enter on other parts. In the brain network, for instance, the net efflux of oxygen from the edges of the plane shown in Fig. 3(F) causes a reduction in oxygen levels there, but oxygenation is improved on the more hypoxic planes above and below (not shown in Fig. 3). These results emphasize the significance of choice of the boundary conditions when estimating hypoxic fraction, an important parameter in predicting the response of tumor tissues to radiation treatment, for example.

Computed PO_2 fields for the rat cremaster muscle network are shown for two different levels of oxygen consumption rate [Figs. 3(G) and 3(H)]. This configuration was simulated using the infinite-domain solution. In this method, the computed PO_2 field extends beyond the defined tissue domain (indicated by the heavy dashed lines), although predicted PO_2 levels outside the domain do not reflect the effects of oxygen sources and sinks lying beyond the tissue domain. Results are shown for two rates of oxygen consumption, 4 and 10 cm^3O_2 $(100\ cm^3)^{-1}$ min^{-1}. At the lower consumption rate [Fig. 3(G)], all the tissue is well-oxygenated and gradients in PO_2 are relatively shallow. At the higher consumption rate, predicted tissue PO_2 levels drop below 1 mmHg in regions between vessels and steep gradients in PO_2 are seen around points of high PO_2, which represent locations where well-oxygenated vessels intersect the planar slice used. In these simulations, PO_2 levels on the boundaries of the tissue domain, as indicated in Fig. 3(G) and 3(H), do not differ systematically from those in the interior of the domain, and cover a similar range of values. In the simulations for this vascular geometry, using a standard 2 GHz personal computer, the computation of the Green's function took 2 min and the computation of the source and sink strengths took 15 min for a sequence of consumption rates starting at 2 cm^3O_2 $(100\ cm^3)^{-1}$ min^{-1} and increasing in steps of 2 to 10 cm^3O_2 $(100\ cm^3)^{-1}$ min^{-1}. This illustrates the feasibility and efficiency of the

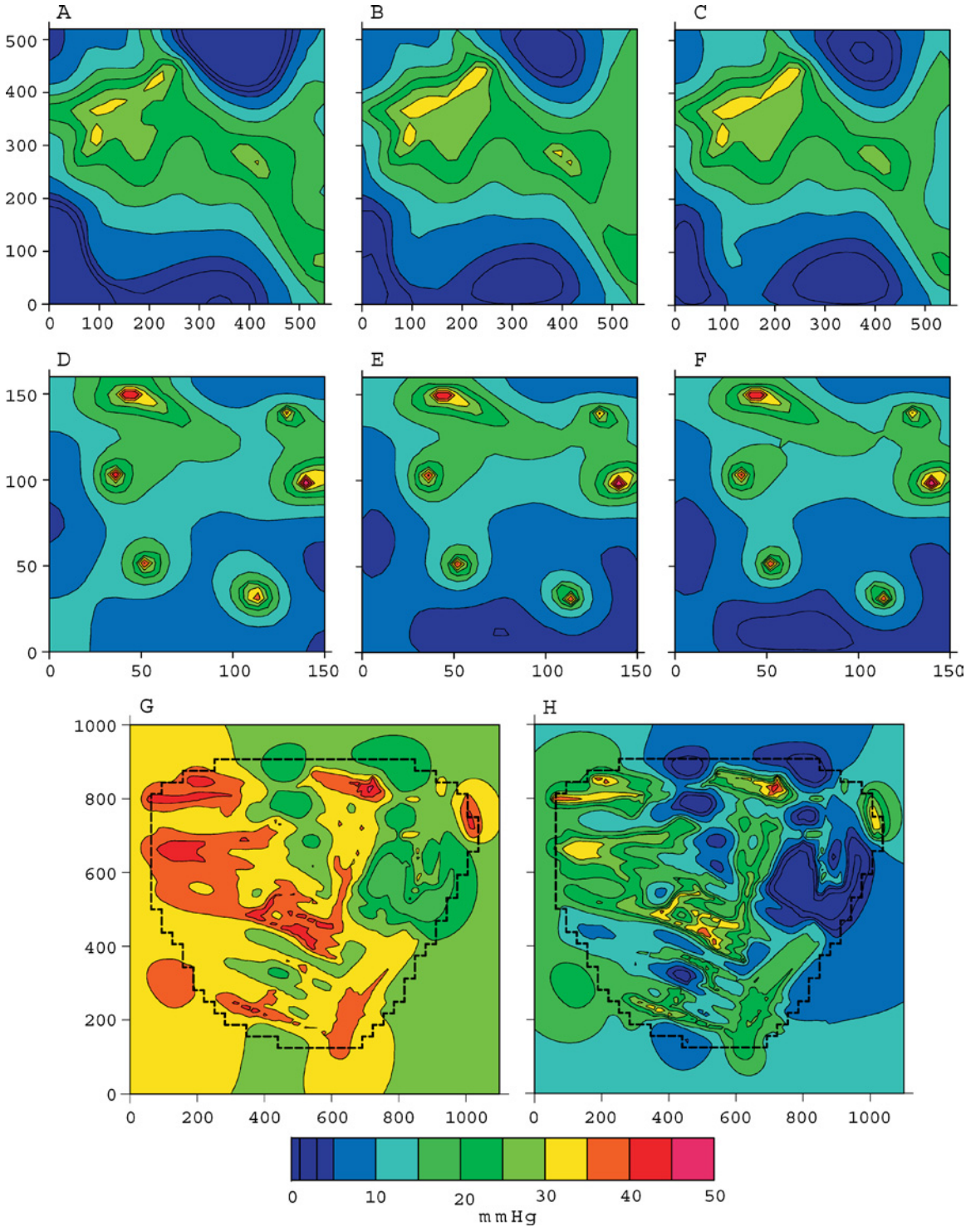

FIGURE 3. Contour plots of PO_2 in planar slices through the rat tumor network (A, B, C), brain network (D, E, F), and cremaster muscle network (G, H). The slices correspond to vertical coordinate values of 125 μm [tumor, as in Fig. 2(A)], 50 μm [brain, as in Fig. 2(B)], and 120 μm [muscle, as in Fig. 2(C)]. For the tumor and brain networks, results are shown for pointwise no-flux solution (A, D), net no-flux solution (B, E), and infinite-domain solution (C, F). For the muscle network, results are shown only for the infinite-domain solution, and for oxygen consumption rates 4 cm^3O_2 $(100\ cm^3)^{-1}$ min^{-1} (G) and 10 cm^3O_2 $(100\ cm^3)^{-1}$ min^{-1} (H). The heavy dashed line shows extent of the oxygen-consuming tissue domain where it intersects the planar slice; oxygen consumption is set to zero outside this region.

TABLE 2. Effect of solution method on estimated hypoxic fraction.

	Rat tumor network (Hypoxic fraction)		Rat brain network (Hypoxic fraction)		
	≤3 mmHg	≤5 mmHg	≤1 mmHg	≤3 mmHg	≤5 mmHg
Pointwise no-flux solution	17.7%	25.0%	7.4%	13.9%	20.2%
Net no-flux solution	11.5%	20.4%	2.2%	10.2%	17.9%
Infinite-domain solution	10.0%	20.3%	1.6%	10.1%	18.1%

method for simulating oxygen transport by relatively complex networks.

DISCUSSION

Simulations of oxygen delivery by vascular networks with realistic three-dimensional geometries have yielded information that cannot easily be obtained from simpler models such as the Krogh cylinder model. For example, such simulations have shown that irregular vascular geometries lead to wider distributions of tissue PO_2, and larger hypoxic regions, than would be expected based on a Krogh model with corresponding vascular density.[32,33] Modeling three-dimensional oxygen diffusion from realistic vascular networks is a relatively demanding computational task. Several strategies have been applied, each with its own advantages and disadvantages. Finite-difference methods can be based directly on a numerical discretization of the governing equations, including any nonlinear effects. Once the solution is obtained, computed values of all desired quantities are available at all points on the computational mesh. However, such methods must use a relatively fine grid to accurately resolve the steep gradients in tissue PO_2 around each vessel, and the number of unknowns can therefore become very large. A further problem that must be overcome is that vessels are not generally aligned with the finite-difference grid, and the application of boundary conditions at the interface between blood and tissue is therefore not straightforward.[1,10] In principle, finite-element methods would be advantageous in this regard.

In the Green's function methods described here, the number of unknowns is greatly reduced by expressing the solution in terms of the source strengths located at a set of points lying along each vessel and throughout the tissue domain. As already discussed, a relatively coarse mesh of points representing tissue consumption can be used without causing substantial error in the computed oxygen field. The reduced number of unknowns makes this method computationally efficient, relative to finite-difference approaches. However, the method is complex to implement, and requires iterative steps to deal with the inherent nonlinearities of the problem, which result from the sigmoidal blood oxyhemoglobin saturation curve and the Michaelis–Menten dependence of oxygen consumption on local tissue PO_2.

Whichever computational approach is used, the problem of choosing appropriate boundary conditions remains. Available sets of data on three-dimensional structures of microvascular networks are restricted to relatively small regions, up to about 1 mm in extent. The actual conditions on tissue PO_2 or oxygen flux on the domain boundaries are unknown. As shown by the results presented here, the distribution of PO_2 and the extent of hypoxia can be substantially affected by the choice of boundary conditions. Use of a non-flux condition, although a seemingly reasonable approach, can exaggerate the occurrence of tissue hypoxia. A no-flux boundary is mathematically equivalent to an internal symmetry plane in the computed PO_2 field. Any region not containing a vascular segment near one or more boundaries is effectively magnified by reflection in these symmetry planes. Near a corner of the cuboidal domain, the presence of three boundaries leads effectively to an eightfold magnification of any vessel-free region, and makes it particularly likely to become hypoxic. In many applications involving cuboidal domains, periodic boundary conditions are a useful alternative. Here, however, use of periodic boundary conditions would result in the appearance of a region of high and rapidly varying PO_2 at any region near the domain boundary opposite to a point where a vessel crosses the domain boundary, because a virtual copy of that vessel would then be present just outside the domain boundary. An advantage of the Green's function approach is that it allows the option of not prescribing a boundary condition, by treating each source and sink as if it was placed in an infinite domain. This approach was previously used by Groebe,[13] who treated each red blood cell as a discrete source of oxygen in an infinite domain. The results presented here suggest that this approach minimizes the artifact associated with boundary conditions, based on the observation that regions of hypoxia are not preferentially located near domain boundaries when the infinite-domain method is used.

In conclusion, Green's function methods have proved useful in simulating oxygen transport to tissue by vascular networks with complex geometries. These methods have been modified to increase their applicability to problems of physiological interest. The problem of assigning boundary conditions remains as a significant issue that must be considered when applying these and other methods. The infinite-domain Green's function method presented here has potential advantages in minimizing effects of the finite extent of the domain on predicted distributions of tissue PO_2.

ACKNOWLEDGMENTS

This study is supported by NIH Grants CA40355, HL34555, and HL70657.

REFERENCES

[1]Beard, D. A. Computational framework for generating transport models from databases of microvascular anatomy. *Ann. Biomed. Eng* 29:837–843, 2001.

[2]Beard, D. A., and J. B. Bassingthwaighte. Modeling advection and diffusion of oxygen in complex vascular networks. *Ann. Biomed. Eng* 29:298–310, 2001.

[3]Beard, D. A., K. A. Schenkman, and E. O. Feigl. Myocardial oxygenation in isolated hearts predicted by an anatomically realistic microvascular transport model. *Am. J. Physiol. Heart. Circ. Physiol.* 285:H1826–H1836, 2003.

[4]Bentley, T. B., H. Meng, and R. N. Pittman. Temperature dependence of oxygen diffusion and consumption in mammalian striated muscle. *Am. J. Physiol.* 264:H1825–H1830, 1993.

[5]Brizel, D. M., B. Klitzman, J. M. Cook, J. Edwards, G. Rosner, and M. W. Dewhirst. A comparison of tumor and normal tissue microvascular hematocrits and red cell fluxes in a rat window chamber model. *Int. J. Radiat. Oncol. Biol. Phys.* 25:269–276, 1993.

[6]Chi, O. Z., H. M. Wei, J. Tse, S. L. Klein, and H. R. Weiss. Cerebral microregional oxygen balance during chronic versus acute hypertension in middle cerebral artery occluded rats. *Anesth. Analg.* 82:587–592, 1996.

[7]Dewhirst, M. W., E. T. Ong, B. Klitzman, T. W. Secomb, R. Z. Vinuya, R. Dodge, D. Brizel, and J. F. Gross. Perivascular oxygen tensions in a transplantable mammary tumor growing in a dorsal flap window chamber. *Radiat. Res.* 130:171–182, 1992.

[8]Duling, B. R., and R. M. Berne. Longitudinal gradients in periarteriolar oxygen tension. A possible mechanism for the participation of oxygen in local regulation of blood flow. *Circ. Res.* 27:669–678, 1970.

[9]Fletcher, J. E. On facilitated oxygen diffusion in muscle tissues. *Biophys. J.* 29:437–458, 1980.

[10]Goldman, D., and A. S. Popel. A computational study of the effect of capillary network anastomoses and tortuosity on oxygen transport. *J. Theor. Biol.* 206:181–194, 2000.

[11]Goldman, D., and A. S. Popel. A computational study of the effect of vasomotion on oxygen transport from capillary networks. *J. Theor. Biol.* 209:189–199, 2001.

[12]Gray, L. H., and J. M. Steadman. Determination of the oxyhaemoglobin dissociation curves for mouse and rat blood. *J. Physiol* 175:161–171, 1964.

[13]Groebe, K. A versatile model of steady state O_2 supply to tissue. Application to skeletal muscle. *Biophys. J.* 57:485–498, 1990.

[14]Hellums, J. D. The resistance to oxygen transport in the capillaries relative to that in the surrounding tissue. *Microvasc. Res.* 13:131–136, 1977.

[15]Hellums, J. D., P. K. Nair, N. S. Huang, and N. Ohshima. Simulation of intraluminal gas transport processes in the microcirculation. *Ann. Biomed. Eng.* 24:1–24, 1996.

[16]Hoofd, L. Updating the Krogh model—assumptions and extensions. In: Oxygen Transport in Biological Systems: Modelling of Pathways from Environment to Cell, edited by S., Egginton and H. F. Ross. Cambridge University Press, 1992, pp. 197–229.

[17]Hoofd, L., J. Olders, and Z. Turek. Oxygen pressures calculated in a tissue volume with parallel capillaries. *Adv. Exp. Med. Biol.* 277:21–29, 1990.

[18]Hoofd, L., Z. Turek, K. Kubat, B. E. Ringnalda, and S. Kazda. Variability of intercapillary distance estimated on histological sections of rat heart. *Adv. Exp. Med. Biol.* 191:239–247, 1985.

[19]Hsu, R., and T. W. Secomb. A Green's function method for analysis of oxygen delivery to tissue by microvascular networks. *Math. Biosci.* 96:61–78, 1989.

[20]Kellogg, O. D. Foundations of Potential Theory. New York: Dover, 1953.

[21]Kimura, H., R. D. Braun, E. T. Ong, R. Hsu, T. W. Secomb, D. Papahadjopoulos, K. Hong, and M. W. Dewhirst. Fluctuations in red cell flux in tumor microvessels can lead to transient hypoxia and reoxygenation in tumor parenchyma. *Cancer Res.* 56:5522–5528, 1996.

[22]Klitzman, B., A. S. Popel, and B. R. Duling. Oxygen transport in resting and contracting hamster cremaster muscles: Experimental and theoretical microvascular studies. *Microvasc. Res.* 25:108–131, 1983.

[23]Krogh, A. The number and the distribution of capillaries in muscle with the calculation of the oxygen pressure necessary for supplying the tissue. *J. Physiol. (Lond.)* 52:409–515, 1919.

[24]Lo, A., A. J. Fuglevand, and T. W. Secomb. Oxygen delivery to skeletal muscle fibers: Effects of microvascular unit structure and control mechanisms. *Am. J. Physiol. Heart Circ. Physiol.* 285:H955–H963, 2003.

[25]Middleman, S. Transport Phenomena in the Cardiovascular System. New York: John Wiley, 1972.

[26]Motti, E. D., H. G. Imhof, and M. G. Yasargil. The terminal vascular bed in the superficial cortex of the rat. An SEM study of corrosion casts. *J. Neurosurg.* 65:834–846, 1986.

[27]Popel, A. S. Theory of oxygen transport to tissue. *Crit. Rev. Biomed. Eng.* 17:257–321, 1989.

[28]Pozrikidis, C., and D. A. Farrow. A model of fluid flow in solid tumors. *Ann. Biomed. Eng.* 31:181–194, 2003.

[29]Pries, A. R., K. Ley, M. Claassen, and P. Gaehtgens. Red cell distribution at microvascular bifurcations. *Microvasc. Res.* 38:81–101, 1989.

[30]Secomb, T. W., and R. Hsu. Analysis of oxygen delivery to tissue by microvascular networks. *Adv. Exp. Med. Biol.* 222:95–103, 1988.

[31]Secomb, T. W., and R. Hsu. Simulation of O_2 transport in skeletal muscle: Diffusive exchange between arterioles and capillaries. *Am. J. Physiol.* 267:H1214–H1221, 1994.

[32]Secomb, T. W., R. Hsu, N. B. Beamer, and B. M. Coull. Theoretical simulation of oxygen transport to brain by networks of microvessels: Effects of oxygen supply and demand on tissue hypoxia. *Microcirculation* 7:237–247, 2000.

[33]Secomb, T. W., R. Hsu, R. D. Braun, J. R. Ross, J. F. Gross, and M. W. Dewhirst. Theoretical simulation of oxygen transport to tumors by three-dimensional networks of microvessels. *Adv. Exp. Med. Biol.* 454:629–634, 1998.

[34]Secomb, T. W., R. Hsu, M. W. Dewhirst, B. Klitzman, and J. F. Gross. Analysis of oxygen transport to tumor tissue by microvascular networks. *Int. J. Radiat. Oncol. Biol. Phys.* 25:481–489, 1993.

[35]Unthank, J. L., J. M. Lash, J. C. Nixon, R. A. Sidner, and H. G. Bohlen. Evaluation of carbocyanine-labeled erythrocytes for microvascular measurements. *Microvasc. Res.* 45:193–210, 1993.

[36]Weiss, R. Parameter-Free Iterative Linear Solvers. Berlin: Akademie Verlag GmbH, 1996.